Real-time Feedback Control of LifeTec Group's Cardiac Biosimulator based on Averaged Hemodynamics

Ivar de Vries * **Mircea Lazar** * **Mattia D'Alessi** **
Marco Stijnen **

* *Electrical Engineering Dept., Eindhoven University of Technology, (e-mails: i.r.d.vries@student.tue.nl, m.lazar@tue.nl)*
** *LifeTec Group, Eindhoven (e-mails: m.dalessi@lifetecgroup.com, m.stijnen@lifetecgroup.com)*

Abstract: LifeTec Group has developed a Cardiac Biosimulator where a dead porcine heart is used to mimic a beating heart in a simulated environment. This is useful for assessment of medical devices or as a training platform for medical professionals. The research presented aims at extending this simulator by designing feedback controllers for the time-averaged relevant pressures and flow, which reduces the startup time and potentially increases stability of the simulator. To achieve this, both the continuous and time-averaged models of the simulator are presented together with their state-space representations. The proposed controller consists of three independent PI controllers, which are presented along with simulation and measurement results and show promising system performance. Lastly, the controller implementation was tested on the Biosimulator with a pathological heart (Mitral prolapse), which showed no significant decrease in performance compared to the physiological heart.

Keywords: Cardiac Biosimulators, Model formulation, Average models for electrical circuits, Control of physiological variables, Digital PID, *ex vivo* platform, beating heart

1. INTRODUCTION

LifeTec Group has developed a Cardiac Biosimulator (CBS) platform (Fig. 1) in which a dead porcine heart is placed (up to a full day) in a simulated physiological environment and heart movement is replicated by means of an external pump. This creates a highly realistic setting for functionality and feasibility assessment for surgical interventional devices and procedures as well as a realistic training platform for medical professionals (Leopaldi et al., 2018). The CBS simulates a beating heart along with heart wall movement, pulsatile pressures and flow and heart valves opening and closing. Moreover, the CBS allows for direct endoscopic visualization of the heart valves since water, rather than blood, can be used. A clinically relevant parameter is the moving average of the pulsatile pressures and flows, which is the focus of this research. Automated control of the averaged signals in the CBS increases the adaptability of the platform, decreases startup time and potentially increases the realism of the simulator. Special care should be taken due to the changing nature of the setup; hearts of different sizes, from different animals and with pathologies can be used in the CBS. This gives the CBS a wide range of applicability but also gives rise to changes in system dynamics for which the desired controller should be robust. Moreover, due to the wide range of applications in which the Biosimulator is used, it is preferred to have a control system architecture which allows control of a subset of the pressures and flow as well.

Fig. 1. A picture of the Cardiac Biosimulator platform showing the simulated environment (middle), endoscopic visualization of the valves (top) and visualization of pressures and flow (right).

Even though models of the human cardiovascular system are readily available (Abdolrazaghi et al., 2010; Magosso and Ursino, 2004) and the heart's behaviour has been described using state-space models (Monzon et al., 2010), these models are not directly applicable due to significant differences between the CBS and the human cardiovascular system. As a consequence, efforts in feedback control of cardiovascular models/mechanical simulators (Uemura et al., 2006; Wu et al., 2007) do not apply and a tailored solution was necessary. Moreover, this research aims at feedback control of the time-averaged hemodynamics in a complex situation where conventional state-space aver-

aging techniques fail. Inspired by power converter control, this challenge was ultimately solved by deriving an average equivalent circuit model.

This paper aims at deriving a feedback control architecture for regulating the time-averaged aortic and left-atrial pressures and cardiac output in the CBS for a healthy heart. To achieve this, continuous and time-averaged models of the CBS are derived together with a control implementation based on the averaged model. After simulation, the controller is tested in real life experiments on the CBS with a healthy and pathological heart (Mitral prolapse). Promising performance is obtained for both simulations and experiments.

Table 1. The duality between the fluid and electrical domain as proposed by (Creigen et al., 2007) and (Blom, 2004), with fluid domain units given in clinically relevant units

Fluid domain		Electrical domain	
Quantity	Unit	Quantity	Unit
Pressure	mmHg	Voltage	V
Flow	ml/s or l/min	Current	A or C/s
Volume	ml	Charge	C
Resistance	mmHg·s/ml	Resistance	Ω or V/A
Compliance	ml/mmHg	Capacitance	F or C/V

2. MODELLING OF THE CBS

Using the duality between the fluid and electrical domain as given in Table 1, an electrical model of the CBS was constructed based on (LifeTec Group, 2019), (Manoliu, 2016), (Blom, 2004), and (Beard, 2012) and is given in Fig. 2a. The relation between the electrical circuit elements in the circuit model and their CBS components is given in Table 2. The sinusoidal current source i_H causes the 2 diodes D_M and D_A to open and close, resulting in characteristic pulsatile voltages and currents. Since inertance can be neglected in models of human circulation (Beard, 2012) and the inertance (as calculated based on (Blom, 2004)) in the CBS is at least 1000 times smaller than that in the human body, inertance is omitted in the developed CBS model.

The goal is to control the moving average of the signals v_{LAP} (Left-Atrial pressure), v_A (Aortic pressure) and i_{R_S} (Systemic flow) via the inputs i_C, i_H and R_S. From Fig. 2 it is clear that the relation between i_{R_S} and v_A is

$$i_{R_S} = \frac{v_A}{R_C + R_S}, \tag{1}$$

which relates the resistance R_S to the input references. Because of this static relationship between v_A and i_{R_S}, the state-space models presented hereafter will focus on the 2 voltages v_{LAP} and v_A only. Under physiological conditions, $v_{LAP}(t) < v_A(t)$ at all times such that the diodes will never conduct simultaneously. As described by (Jain et al., 2014), this gives three possible modes:

(1) the isovolumic mode: both diodes are non-conducting
(2) the ejection mode: only D_A (the Aortic valve) is open
(3) the filling mode: only D_M (the Mitral valve) is open.

The system switches in the order $1 \rightarrow 2 \rightarrow 1 \rightarrow 3$, which means that the isovolumic state is reached twice each period.

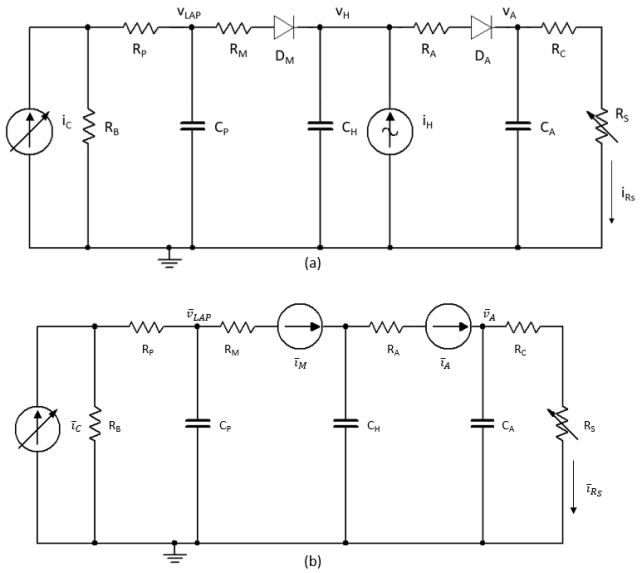

Fig. 2. (a) Circuit model representation of the CBS and its (b) time-averaged equivalent.

2.1 Continuous state-space model

For $k \in \{1, 2, 3\}$ representing the isovolumic, ejection and filling phase respectively, a signal $c_k(t) \in \{0, 1\}$ and matrices $\mathbf{A_k}(R_S)$ can be used to represent the system in Fig 2a by a switched state-space model. This model is given by the equations

$$\begin{aligned} \frac{d\mathbf{x}}{dt} &= \Big[c_1^1(t)\mathbf{A_1}(R_S) + c_2(t)\mathbf{A_2}(R_S) + c_1^2(t)\mathbf{A_1}(R_S) \\ &\quad + c_3(t)\mathbf{A_3}(R_S)\Big]\mathbf{x}(t) + \mathbf{B}\mathbf{u}(t) \\ \mathbf{y}(t) &= \mathbf{C}\mathbf{x}(t), \end{aligned} \tag{2}$$

where $c_1^1(t)$ and $c_1^2(t)$ denote the first and second isovolumic phases respectively. Since the system can only be in one mode at a any time it holds that

$$c_1^1(t) + c_2(t) + c_1^2(t) + c_3(t) = 1 \quad \forall t. \tag{3}$$

The matrices $\mathbf{B}$ and $\mathbf{C}$ do not depend on the mode of the system and are thus constant for all time. For the output, state and control vectors are defined as:

$$\begin{aligned} &\mathbf{x}(t) = [v_H(t)\ v_{LAP}(t)\ v_A(t)]^T,\ \mathbf{u}(t) = [i_H(t)\ i_C(t)]^T, \\ &\mathbf{y}(t) = [v_{LAP}(t)\ v_A(t)]^T. \end{aligned} \tag{4}$$

Table 2. Circuit elements present in Fig. 2 and CBS counterparts

Circuit	CBS component
i_C	Flow generated by circulation pump
R_B	Bypass resistance (manually set)
R_P	Resistance arising from tubing before the heart
C_P	The compliance present before the heart
R_M	Mitral valve resistance
D_M	Mitral valve
C_H	The compliance of the heart
i_H	Sinusoidal flow generated by piston pump
R_A	Atrial valve resistance
D_A	Atrial valve
C_A	The compliance after the heart
R_C	Resistance arising from tubing after the heart
R_S	Controlled afterload resistance

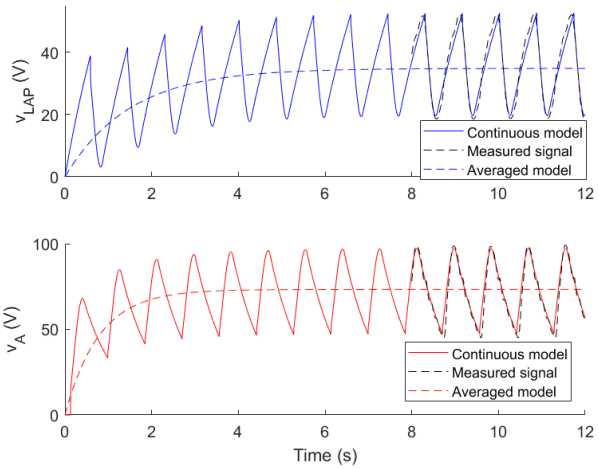

Fig. 3. Simulation results for the continuous and average models starting from zero initial conditions. Signals measured on the CBS are shown from 8 to 12 seconds.

The matrices of the state-space model are given by

$$\mathbf{A_1}(R_S) = \begin{bmatrix} 0 & 0 & 0 \\ 0 & \dfrac{-1}{(R_B+R_P)C_P} & 0 \\ 0 & 0 & \dfrac{-1}{(R_C+R_S)C_A} \end{bmatrix}$$

$$\mathbf{A_2}(R_S) = \begin{bmatrix} \dfrac{-1}{R_A C_H} & 0 & \dfrac{1}{R_A C_H} \\ 0 & \dfrac{-1}{(R_B+R_P)C_P} & 0 \\ \dfrac{1}{R_A C_A} & 0 & \dfrac{-R_A-R_C-R_S}{R_A(R_C+R_S)C_A} \end{bmatrix}$$

$$\mathbf{A_3}(R_S) = \begin{bmatrix} \dfrac{-1}{R_M C_H} & \dfrac{1}{R_M C_H} & 0 \\ \dfrac{1}{R_M C_P} & \dfrac{-R_M-R_B-R_P}{R_M(R_B+R_P)C_P} & 0 \\ 0 & 0 & \dfrac{-1}{(R_C+R_S)C_A} \end{bmatrix}$$

$$\mathbf{B} = \begin{bmatrix} \dfrac{1}{C_H} & 0 \\ 0 & \dfrac{R_B}{(R_B+R_P)C_P} \\ 0 & 0 \end{bmatrix} \quad \mathbf{C} = \begin{bmatrix} 0 & 1 & 0 \\ 0 & 0 & 1 \end{bmatrix}.$$

Fig. 3 shows a simulation result for the switched state-space model starting from zero initial conditions. A measurement on the CBS is shown from 8 to 12 seconds for visual comparison and shows great resemblance for both v_{LAP} and v_A. The simulated signal has an Root-Mean-Square Error (RMSE) of 6.9% and 6.3% with respect to the measured average steady-state values for v_{LAP} and v_A respectively.

2.2 Time-averaged state-space model analysis

The moving average operator of any signal $x(t)$ over a period T can be defined as

$$\bar{x}(t) = \frac{1}{T}\int_{t-T}^{t} x(\tau)d\tau. \tag{5}$$

Applying this to the voltages and currents gives the averaged equivalent circuit given in Fig. 2b. Compared to Fig. 2a, the sinusoidal current together with the two diodes are replaced by two current sources representing the average currents trough both diodes. As described by (Guyton, 1955), these averaged currents are equal in steady state, which results in $\bar{i}_M(t) = \bar{i}_A(t)$.

After linearization around a steady-state operating point by assuming $\bar{i}_M(t) = \bar{i}_A(t)$ for all times, the averaged state-space model (based on (Corradini et al., 2015)) is

$$\frac{d\bar{\mathbf{x}}}{dt} = \mathbf{A_A}(R_S)\bar{\mathbf{x}}(t) + \mathbf{B_A}\bar{\mathbf{u}}(t), \quad \bar{\mathbf{y}}(t) = \mathbf{C_A}\bar{\mathbf{x}}(t), \tag{6}$$

with the output, state and control vectors defined as

$$\begin{aligned} \bar{\mathbf{y}}(t) = \bar{\mathbf{x}}(t) &= \left[\bar{v}_{LAP}(t)\ \bar{v}_A(t)\right]^T, \\ \bar{\mathbf{u}}(t) &= \left[\bar{i}_M(t)\ \bar{i}_C(t)\right]^T \end{aligned} \tag{7}$$

and the matrices are given by

$$\mathbf{A_A}(R_S) = \begin{bmatrix} \dfrac{-1}{(R_B+R_P)C_P} & 0 \\ 0 & \dfrac{-1}{(R_C+R_S)C_A} \end{bmatrix},$$

$$\mathbf{B_A} = \begin{bmatrix} \dfrac{-1}{C_P} & \dfrac{R_B}{(R_B+R_P)C_P} \\ \dfrac{1}{C_A} & 0 \end{bmatrix}, \quad \mathbf{C_A} = \begin{bmatrix} 1 & 0 \\ 0 & 1 \end{bmatrix}.$$

Simulation results for this averaged state-space model are given in Fig. 3 and give a steady-state error of 0.002% and 0.012% between the numerical and simulated moving average for v_{LAP} and v_A respectively. The controllability matrix for the averaged state-space model is given by

$$C = [\mathbf{B_A}\ \mathbf{A_A}\mathbf{B_A}] = \begin{bmatrix} \dfrac{-1}{C_P} & \dfrac{R_B}{(R_B+R_P)C_P} & \dfrac{1}{(R_B+R_P)C_P^2} & \dfrac{-1}{(R_B+R_P)^2C_P^2} \\ \dfrac{1}{C_A} & 0 & \dfrac{-1}{(R_C+R_S)C_A^2} & 0 \end{bmatrix}$$

and has rank 2 for $R_B \neq 0$. Since this is true by design, the system is controllable for all R_S.

Since the control inputs of the continuous and averaged state-space models are not identical, a relation between the two should be found in order to use the averaged state-space model to design a controller for the CBS. In particular, a relation between the sinusoidal current $i_H(t)$ and the average flow $\bar{i}_M(t)$ should be found. The sinusoidal current $i_H(t)$ is generated by the CBS and can be controlled by setting the Stroke Volume (SV) in a LabVIEW environment, which then generates the current

$$i_H(t) = SV \cdot \alpha \sin\left(2\pi\frac{HR}{60}t\right), \tag{8}$$

with α a constant and HR the heart rate in Beats per minute (BPM). Since no analytical solution relating $\bar{i}_M$ to SV could be found, the relation between the two was found empirically as

$$SV = \beta \cdot \bar{i}_M - \left(\gamma - \delta\sqrt{R_C+R_S}\right) \cdot i_C R_B \tag{9}$$

with β, γ and δ constants. Values for the mentioned constants are given in Appendix A.

3. CONTROLLER DESIGN AND SIMULATION

Looking at the system matrix $\mathbf{A_A}$ and input matrix $\mathbf{B_A}$, it can be seen that the output $\bar{v}_A(t)$ is directly

controlled by the input $\bar{i}_M(t)$, while the output $\bar{v}_{LAP}(t)$ depends on both elements of the input vector. Due to hardware limitations, the current $\bar{i}_M(t)$ (controlled by the SV) can only be updated at frequencies of 0.25 Hz, whereas the second input $\bar{i}_C(t)$ can be updated at 100 Hz. Because of this, control of both outputs was decoupled and two independent PI-controllers were implemented. As a consequence of this decoupling, any update on $\bar{i}_M(t)$ acts as a disturbance on the output v_{LAP}, which should be corrected by the faster controller.

Fig. 4 gives an overview of the proposed control system architecture for the whole system, which shows the division in the three independent controllers:

- The *Cardiac output controller* takes the Aortic pressure (v_A) as a reference and controls the amplitude of the sinusoidal current i_H by setting SV;
- The *Afterload controller* takes the ratio between the Aortic pressure and the flow ($\frac{v_A}{i_{R_S}}$) as a reference and directly controls the afterload resistance;
- The *Preload controller* takes the Left-Atrial pressure (v_{LAP}) as a reference and adjusts the current i_C via a PWM duty-cycle.

To enhance the performance of the system, feed-forward for the slower *Cardiac output controller* was implemented based on (Guyton, 1955) which gives the Cardiac Output (CO) as the product of stroke volume and heart rate. Since the CBS runs at a heart rate of 70 BPM for virtually all use cases, the heart rate is assumed static at 70 BPM in this research.

The general discrete PI controller was implemented by the so-called velocity form given by (Djamel et al., 2019) and (Wang, 2020) as

$$u[k] = K_p\big(e[k] - e[k-1]\big) + u[k-1] + K_i e[k], \qquad (10)$$

where $u[k]$ is the control signal, $e[k]$ is the error with respect to the reference and k gives the sampled time index. This velocity form implementation is obtained from the discrete-time PID implementation

$$u[k] = K_p e[k] + K_i \sum_{n=1}^{k} e[k] \qquad (11)$$

by subtracting $u[k-1]$ from $u[k]$ and was chosen because of its lower computational and memory intensiveness compared to the traditional implementation.

The afterload resistance R_S is controlled by a stepper motor which regulates the radius of a tube segment. Because of the changing nature of the setup, a lookup table relating the position and resistance cannot be constructed and control should be implemented to arrive at the correct resistance $R_C + R_S$. Since the stepper motor will not move unless an input is given, it has memory, similar to the term $u[k-1]$ in equation (10). Therefore taking steps proportional to the error results in a purely integral controller.

Since the ratio between the desired aortic pressure and flow concerns a static relation, this controller can work independently of the other two controllers. The delay caused by the flow sensor was measured to be 0.11 seconds and arises from the calculations done in the flow sensor software. This controller was chosen to run at 0.25 Hz along with the Cardiac output controller to account for the delay caused by the pressure sensor. The afterload controller was deactivated for errors in the afterload resistance of less than 5% to prevent oscillations caused by measurement noise, essentially allowing a 5% error in i_{R_S}. Tuning of the afterload controller was done on the real-life setup since the afterload resistance itself could not be simulated.

Fig. 5 shows the simulated control of the switched state-space model via the moving average over one heart beat period. In order of priority, the controllers were tuned for

(1) Robustness to noise and changing system dynamics;
(2) Minimal overshoot in the Aortic pressure (v_A);
(3) Fast rise and settling times.

The simulation results shown in Fig. 5 clearly show interaction between the two control loops, which is caused by the relation given in the average state-space model and the calculation of $\bar{i}_M$ given in equation (9). As can be seen, the disturbances are typically compensated within 10 seconds. This simulation does not include simultaneous control of the afterload resistance, but the controllers were tuned for the whole range of relevant afterload resistance values.

4. EXPERIMENTS ON THE CBS

The designed controllers were tested on the CBS, during which it was found that the pump generating the sinusoidal current i_H has limitations causing the pump to occasionally stall for one or two seconds after receiving an update in the sine wave amplitude. This happens at purely random moments and has severe consequences for the system performance as it slows down the settling time and leads to an overshoot in the Aortic pressure due to the integral action of the controller.

Fig. 6 shows the pressures and resistance measured on the CBS, which compared to Fig. 5, show a high overshoot and a long settling time. This is caused by the stalling of the pump, the simultaneous control of the afterload and measurement noise, which were not taken into account during simulations. The interaction between the loops is visible as well and it is successfully compensated by the independent controllers.

Table 3 shows a comparison between the simulated and measured overshoots, which clearly shows the difference between simulation and measurements.

An important use case of the CBS is Mitral valve prolapse, during which the diode D_M in Fig. 2a does not close properly and a small amount of current is allowed to flow in the blocking direction. This changes the system dynamics and experiments were done to reveal to which extent the average model and consequently the controller implementation are still valid. Fig. 7 shows measurement results for a heart with typical Mitral prolapse for use cases at LifeTec Group, which compared to the measurement results shown in Fig. 6 shows faster settling time and less overshoot. This is presumably caused by less stalling of the pump and a faster settling time of the afterload resistance. Compared to a healthy heart, Table 3 also shows less overshoot for the cardiac and afterload controllers, while the overshoot for the preload controller has increased.

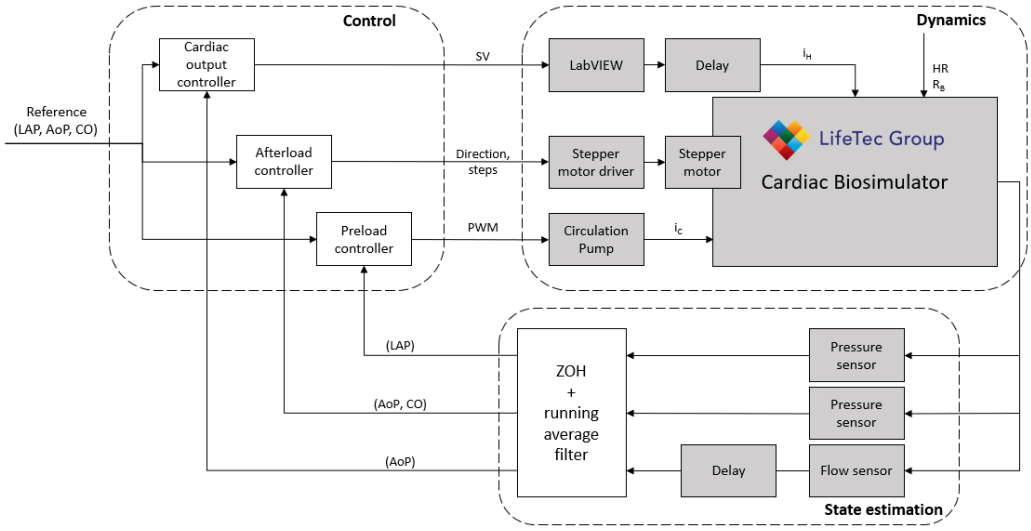

Fig. 4. An overview of the proposed control system architecture for the CBS, white blocks are added during this research.

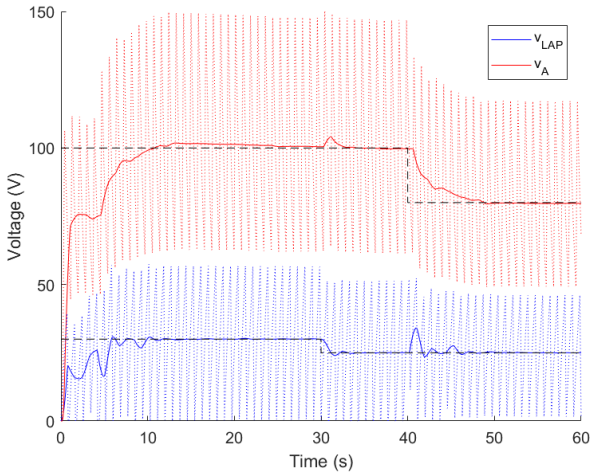

Fig. 5. Simulation results for the two independent control loops showing the average voltage along with the continuous voltage (dotted) and the reference values (dashed).

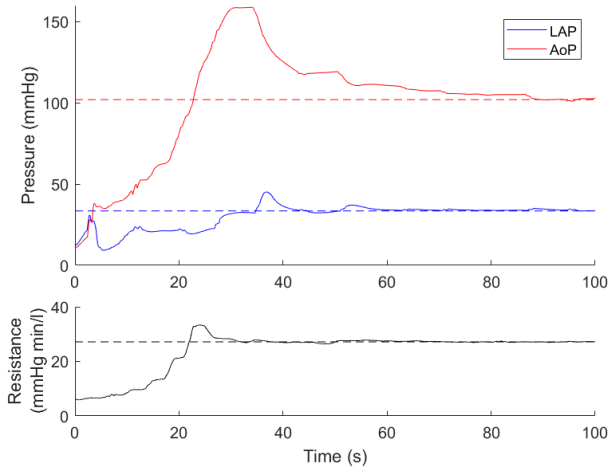

Fig. 6. Measurement results for the three control loops showing the average pressures along with their reference values (top) and the total afterload resistance along with its reference (bottom). Stalling of the pump occurs at around 10 seconds.

5. CONCLUSIONS AND RECOMMENDATIONS

This paper proposed a control system implementation tailored to the Cardiac Biosimulator developed by LifeTec Group. To this extent, continuous and time-averaged state-space models were presented which show good agreement with each other and real-life measurements. The proposed control system architecture consists of three independent PI-controllers, which allows the use of a subset of the three controllers when desired. This makes the implementation more flexible to the changing requirements of the Cardiac Biosimulator when used for different applications. Furthermore, the implemented controllers proved stable for changing system dynamics and the occurrence of typical Mitral valve prolapse does not significantly reduce the system performance. Differences between the simulated and measured control were caused by hardware limitations of the CBS, simultaneous control of the afterload resistance and the presence of measurement noise. Future research can be done to adjust the controller for more demanding use cases (e.g. hypertension) and the controller might be adjusted to show behavior closer to that of the human heart. Especially the latter will show a large increase in the realism of the Cardiac Biosimulator.

Table 3. Simulated and measured overshoots for the different controllers

Controller	Simulated	Healthy	Prolapse
Preload	2.83%	34.8%	61.4%
Cardiac output	1.9%	55.8%	38%
Afterload	n/a	22.7%	9.5%

6. CONFLICT OF INTEREST STATEMENT

M. D'Alessi and M. Stijnen are employees of LifeTec Group BV.

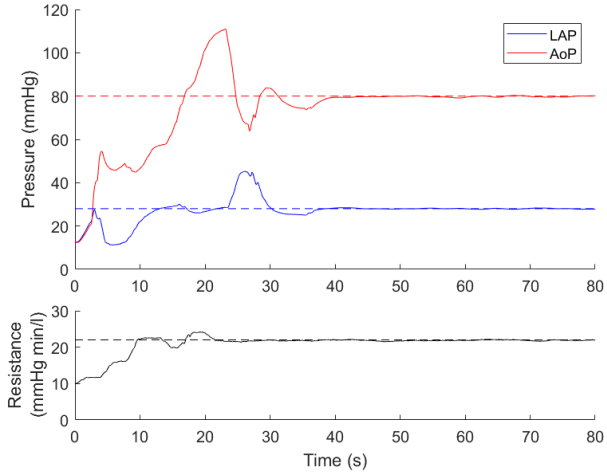

Fig. 7. Measurement results for a heart with typical Mitral prolapse showing the average pressures with their reference values (top) and the total afterload resistance with its reference (bottom). Stalling of the pump occurs between 25 and 30 seconds.

7. ACKNOWLEDGEMENTS

This research was partly funded by the Stimuleringsfonds grant from Metropoolregio Eindhoven. LifeTec Group gratefully acknowledges this financial support.

REFERENCES

Abdolrazaghi, M., Navidbakhsh, M., and Hassani, K. (2010). Mathematical modelling and electrical analog equivalent of the human cardiovascular system. *Cardiovascular Engineering*, 10(2), 45–51. doi:10.1007/s10558-010-9093-0.

Beard, D. (2012). Cardiovascular systems simulation. In *Biosimulation: Simulation of Living Systems*, 105–144. Cambridge University Press, Cambridge.

Blom, J. (2004). *Monitoring of respiration and circulation*. 1. CRC Press.

Corradini, L., Maksimović, D., Mattavelli, P., and Zane, R. (2015). Continuos-time averaged modeling of DC-DC converters. In *Digital Control of High-Frequency Switched-Mode Power Converters*, 13–50. John Wiley & Sons, Inc. doi:10.1002/9781119025498.

Creigen, V., Ferracina, L., Hlod, A., Mourik, S.V., Sjauw, K., Rottschafer, V., Vellekoop, M., and Zegeling, P. (2007). Modeling a Heart Pump. *Proceedings of the 58st European Study Group Mathematics with Industry*, 7–26.

Djamel, O., Dhaouadi, G., Youcef, S., and Mahmoud, M. (2019). Hardware Implementation of Digital PID Controller for DC-DC Boost Converter. *Proceedings - 2019 4th International Conference on Power Electronics and their Applications, ICPEA 2019*, 25–27. doi:10.1109/ICPEA1.2019.8911129.

Guyton, A.C. (1955). Determination of cardiac output by equating venous return curves with cardiac response curves. *Physiological reviews*, 35(1), 123–129. doi:10.1152/physrev.1955.35.1.123.

Jain, K., Pal, T., and Maka, S. (2014). Stability issues in a cardiovascular circulation. *IEEE TechSym 2014 - 2014 IEEE Students' Technology Symposium*, 414–419. doi:10.1109/TechSym.2014.6808087.

Leopaldi, A.M., Wrobel, K., Speziali, G., van Tuijl, S., Drasutiene, A., and Chitwood, W.R. (2018). The dynamic cardiac biosimulator: A method for training physicians in beating-heart mitral valve repair procedures. *Journal of Thoracic and Cardiovascular Surgery*, 155(1), 147–155. doi:10.1016/j.jtcvs.2017.09.011.

LifeTec Group (2019). Cardiac Biosimulator operating manual.

Magosso, E. and Ursino, M. (2004). Effects of cardiovascular parameter changes on heart rate variability: Analysis by a mathematical model of short-term cardiovascular regulation. *Annual International Conference of the IEEE Engineering in Medicine and Biology - Proceedings*, 26 VI, 3905–3908. doi:10.1109/iembs.2004.1404092.

Manoliu, V. (2016). Modeling cardiovascular hemodynamics in a model with nonlinear parameters. In *2015 E-Health and Bioengineering Conference, EHB 2015*, November, 1–4. Iasi, Romania. doi:10.1109/EHB.2015.7391407.

Monzon, J.E., Pisarello, M.I., Picaza, C.A., and Veglia, J.I. (2010). Dynamic modeling of the vascular system in the state-space. *2010 Annual International Conference of the IEEE Engineering in Medicine and Biology Society, EMBC'10*, 2612–2615. doi:10.1109/IEMBS.2010.5626612.

Uemura, K., Kamiya, A., Shimizu, S., Shishido, T., Sugimachi, M., and Sunagawa, K. (2006). Comprehensive physiological cardiovascular model enables automatic correction of hemodynamics in patients with acute life-threatening heart failure. *Annual International Conference of the IEEE Engineering in Medicine and Biology - Proceedings*, 198–201. doi:10.1109/IEMBS.2006.259935.

Wang, L. (2020). Implementation of PID Controllers. In *PID Control System Design and Automatic Tuning using MATLAB/Simulink*, chapter 4, 113–138. John Wiley & Sons Ltd. doi:10.1002/9781119469414.ch4.

Wu, Y., Allaire, P.E., Tao, G., and Olsen, D. (2007). Modeling, estimation, and control of human circulatory system with a left ventricular assist device. *IEEE Transactions on Control Systems Technology*, 15(4), 754–767. doi:10.1109/TCST.2006.890288.

Appendix A. VALUES USED IN THIS RESEARCH

Table A.1. Controller values used in this paper

Control	Variable	Value
Cardiac output	freq.	0.25 Hz
	K_p	0.1
	K_i	0.063
After load	freq.	0.25 Hz
	K_p	0
	K_i	1
Preload	freq.	100 Hz
	K_p	0.008
	K_i	0.006

Table A.2. Parameter values used for the relation between the continuous and average models

Parameter	Value
α	π*HR/60
β	2.57
γ	0.3845
δ	0.1701